Analyst

Check for updates

Online monitoring of epithelial barrier kinetics and cell detachment during cisplatin-induced toxicity of renal proximal tubule cells†

Yuji Takata, [ID] Ramin Banan Sadeghian, [ID] Kazuya Fujimoto [ID] and Ryuji Yokokawa [ID] *

Real-time and non-invasive assessment of tissue health is crucial for maximizing the potential of microphysiological systems (MPS) for drug-induced nephrotoxicity screening. Although impedance has been widely considered as a measure of the barrier function, it has not been incorporated to detect cell detachment in MPS with top and bottom microfluidic channels separated by a porous membrane. During cell delamination from the porous membrane, the resistance between both channels decreases, while capacitance increases, allowing the detection of such detachment. Previously reported concepts have solely attributed the decrease in the resistance to the distortion of the barrier function, ignoring the resistance and capacitance changes due to cell detachment. Here, we report a two-channel MPS with integrated indium tin oxide (ITO) electrodes capable of measuring impedance in real time. The trans-epithelial electrical resistance (TEER) and tissue reactance (capacitance) were extracted from the impedance profiles. We attributed the anomalous initial increase observed in TEER, upon cisplatin administration, to the distortion of tight junctions. Cell detachment was captured by sudden jumps in capacitance. TEER profiles illuminated the effects of cisplatin and cimetidine treatments in a dose-dependent and polarity-dependent manner. The correspondence between TEER and barrier function was validated for a continuous tissue using the capacitance profiles. These results demonstrate that capacitance can be used as a real-time and non-invasive indicator of confluence and will support the accuracy of the drug-induced cytotoxicity assessed by TEER profiles in the two-channel MPS for the barrier function of a cell monolayer.

1. Introduction

Microphysiological systems (MPS) are well suited for applications in nephrotoxicity screening because they can help model the pharmacokinetics and pharmacodynamics of drugs under question, enhancing preclinical efficacy and safety.[1,2] The renal proximal tubules (PTs) happen to be the most sensitive renal organs to nephrotoxicity due to their role in excreting drugs and metabolites.[3,4] This fact highlights the need for PT-MPS as more accurate clinical prediction models for PT nephrotoxicity during drug discovery and early development. Despite the significant requirements in PT-MPS technologies, measurement techniques for toxicological monitoring still rely on traditional methods to detect cellular damage in nephrotoxicity.[5,6] These methods are labor-intensive, often disruptive, and, most critically, only provide end-point data.[7]

Of late, there is an increasing demand for the utilization of impedance measurement techniques in MPS for *in vitro* toxicology studies.[8,9] These methods offer several advantages, including high sensitivity, label-free, and real-time measurements.[10] Real-time measurements may facilitate the acquisition of information on cell function and pharmacodynamic drug responses with high temporal resolution.[5,11] At least two parameters can be derived from the impedance profiles: the trans-epithelial electrical resistance (TEER) of the cell monolayer, which is an indicator of the integrity of the tight junction barrier and correlates with tissue quality,[12] and the capacitance, which can be related to the total surface area of the cell layer and is indicative of cell behaviors including cell differentiation, attachment or detachment, and cell migration.[13–15] However, the capacitance has not been well integrated in MPS to assess the cellular behaviors owing to the difficulty of electrode location in microfluidic channels.

Department of Micro Engineering, Kyoto University, Kyoto, Japan.
E-mail: yokokawa.ryuji.8c@kyoto-u.ac.jp

Electrical cell–substrate impedance sensing (ECIS) is one of the well-established techniques, or responses to drugs by measuring the impedance of cells adhering to an electrode surface.[13,16–19] However, ECIS systems suffer from a major limitation: the basal side of the cells are inaccessible to drug doses because they are directly attached to the electrode surface. Basal cell access and treatment are essential for the evaluation of certain cell types.[20] Transporters expressed on the basal and apical membranes of the PT play crucial roles in the tubular secretion and reabsorption processes of various drugs.[21] For instance, cisplatin, a notable nephrotoxic anti-cancer drug, is dominantly mediated by organic cation transporter 2 (OCT2) which is expressed on the basolateral membrane of PT epithelial cells.[22,23] Although cisplatin is taken up by endocytosis through an endocytic receptor called low density lipoprotein receptor-related protein 2 (LRP2) expressed at the apical membrane, cisplatin administration into the basolateral side exhibits stronger cytotoxicity than that into the apical side.[24]

A common MPS consists of a porous membrane separating two channels to support a epithelial tissue. Gold electrodes, which are the most commonly used electrode material owing to their characteristics of inertness and biocompatibility, were partially patterned on the cell culture area to facilitate microscopic observation.[9,10] However, the culture area covered by electrodes was insufficient,[25] making it impossible to detect cell detachment that would occur randomly throughout the cell layer, since the capacitance measurement is hindered by non-uniform electric fields.[25,26] Therefore, after the cell detachment, an electric current flows through the acellular area, and the equivalent circuit model is no longer valid in the previously reported impedance measurement in MPS.

In this study, we propose to measure TEER only when cells form a tissue monolayer, whose disruption can be detected by the increase of capacitance owing to the cell detachment from a monolayer tissue. We first established a PT-MPS with integrated indium tin oxide (ITO) electrodes covering the entire culture area. We assessed the expression and structure of the tight junction proteins ZO-1 and claudin-2 (CLDN2) to demonstrate that the measured TEER corresponds to the changes in the barrier function. In addition, we confirmed that the measured variances in capacitance correspond to cell detachment. Finally, a cisplatin-induced nephrotoxicity model was utilized to assess the feasibility of impedance measurements for PT nephrotoxicity screening before cell detachment. Cisplatin is well-characterized for its dose-dependent and cell polarity-dependent toxicity.[27,28]

2. Experimental section

2.1. Device fabrication

The PT-MPS utilized herein is a five-layered structure composed of two glass substrates with two integrated ITO electrodes, two polydimethylsiloxane (PDMS) sheets with a micro-

channel, and a porous PET membrane (Fig. 1A and B). Two isolated ITO electrodes were patterned on glass substrates by sputtering and etching (Fig. 1C). Identical microchannels were created on PDMS sheets by laser cutting (Fig. 1D).

The PDMS sheets were self-adhesively bonded to the glass substrates. The PDMS prepolymer was applied on the edge of the PDMS sheets and baked at 95 °C for 15 min to firmly attach the substrates to the PDMS sheets. Next, a thin layer of the PDMS prepolymer as an adhesive layer was spin coated (2200 rpm, 30 s) on a glass slide (S9111, MATSUNAMI). The layer was transferred to the PDMS sheet by positioning the sheet momentarily on the glass slide. Porous PET membranes (3 μm pore, PET3047100, STERLITECH) were laser cut to sections 18 mm in length and 10 mm in width to cover the straight part of the channel. The membrane was then placed on the bottom PDMS sheet and aligned with the top PDMS sheet on the glass substrate. After successful alignment, the devices were incubated for 3 days at 4 °C and at room temperature for 1 day to cure the PDMS prepolymer. Finally, the medium reservoirs were attached.

2.2. Epithelial cell culture

hTERT-importalized renal proximal tubule epithelial cells (RPTEC, CRL-4031, ATCC) were subcultured in T-25 flasks (90026, TPP) using medium suggested by the manufacturer until reaching 90% confluency. The device membranes were coated on the top side with a cell adhesion promoter (FNC coating mix, 0407, Funakoshi), and then the devices were incubated at 37 °C for 1 min. Before seeding, RPTECs in the flasks were trypsinized (204-16935, Lonza), suspended at 3×10^6 cells per 100 μL, and then seeded on the membrane of the apical channel (Fig. 1E). Renal epithelial cell growth medium (REGM, CC-3190, Lonza) was used for device culture. Gentamicin and amphotericin from the kit were replaced with 100 U mL^{-1} penicillin and 100 μg mL^{-1} streptomycin (09367-34, Gibco). The RPTECs maintained the expression of ZO-1 and OCT2 after the epithelial tissue was matured on day 8 (Fig. 1F).

2.3. Drug solutions

Cisplatin (033-20091, Fujifilm) and cimetidine (C1252-25G, TCI) were dissolved in Dulbecco's phosphate-buffered saline (DPBS, 14040-133, Gibco) and dimethyl sulfoxide (DMSO, 047-29353, Fujifilm) vehicles at concentrations of 1 mM and 1 M, respectively, and stored for later use. The stock solutions were diluted to the working concentration in REGM. The vehicle control contained an equivalent amount of the stock solution in REGM.

2.4. Impedance measurements

TEER profiles were first measured manually using Millicell ERS-2 with a chopstick-like electrode (MERS00002, Merck Millipore) in a laminar flow hood to prevent contamination. For the control experiment, RPTECs were cultured on 24-well transwell inserts (3 μm pore filters, PTSP24H48, Merck
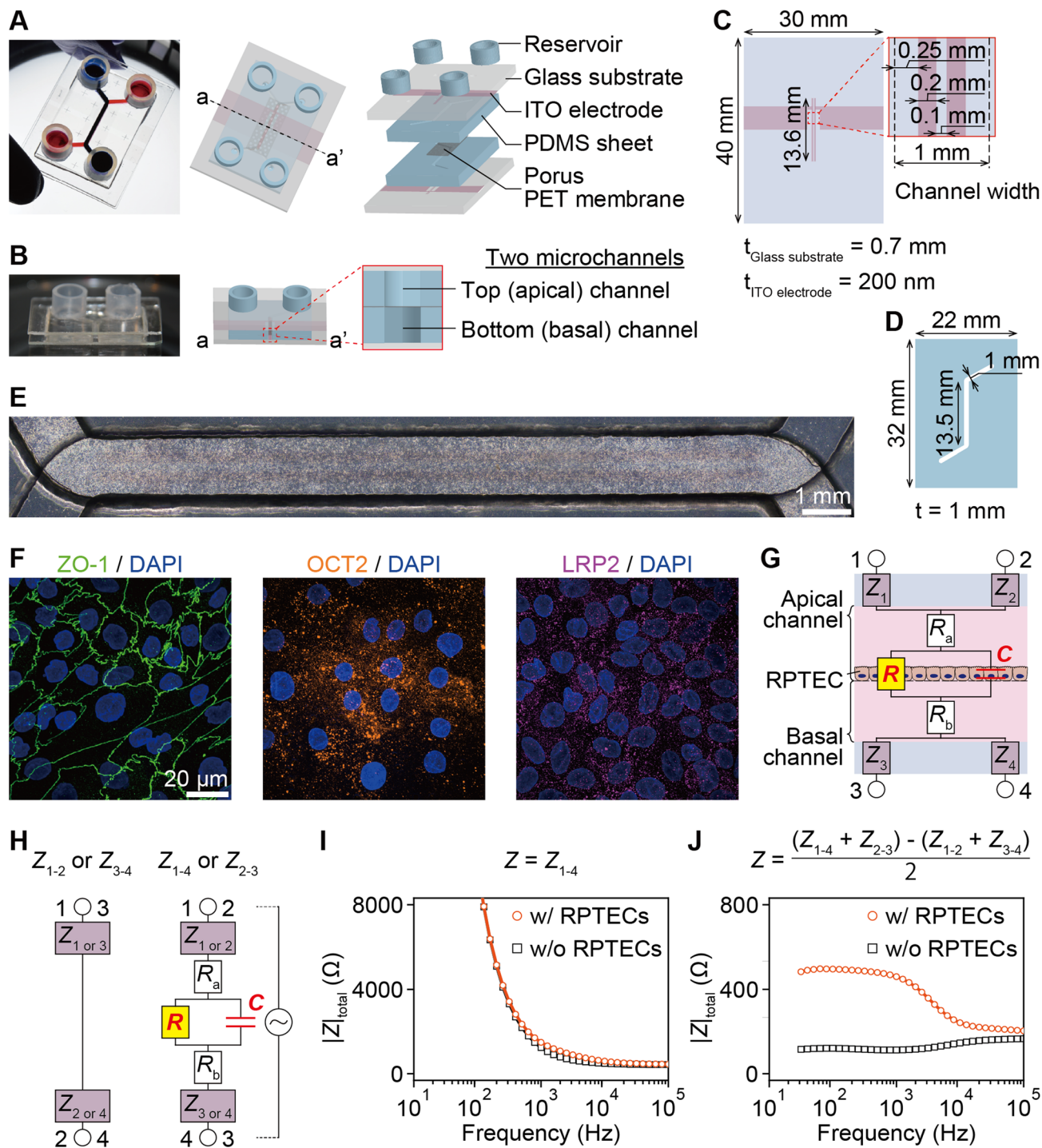
Fig. 1 Proximal tubule device design and the corresponding equivalent electrical circuit model. A. A photograph of the assembled device and a schematic exploded view, consisting of reservoirs embedded to store culture medium and the five-layered structure composed of two glass substrates with ITO electrodes, two PDMS sheets with microchannels, and the porous PET membrane. B. A photograph of the cross-sectioned device and a schematic cross-sectional view with top (apical) and bottom (basal) channels. C. Dimensions of the glass substrates (light blue) and the ITO electrodes (pink) patterned on the glass substrates. D. Dimensions of the PDMS sheets with engraved microchannels. E. Bright field image of the entire channels after RPTECs were seeded. Scale bar = 1 mm. F. Fluorescence z-stack images of RPTECs stained with ZO-1 (green), OCT2 (orange), and LRP2 (magenta). Nuclei counter-stained with DAPI (blue). Scale bar = 20 μm. G. Schematic illustration of a cross section of the device and the equivalent electrical circuit of the entire system with impedance of the four electrodes (Z_1, Z_2, Z_3 and Z_4), resistance of the medium in the apical channel (R_a) and in the basal channel (R_b), the trans-epithelial electrical resistance (TEER, R), and the capacitance of the cell monolayer (C). H. Equivalent circuits illustrating independent measurements of impedance from the circuit in G. Impedance was measured independently four times through electrodes 1-2, 3-4, 1-4, and 2-3. Examples of impedance spectra for a device with RPTECs and a device without RPTECs (I) measured among the electrodes 1–4 and (J) calculated from measurements at the four electrodes.

Millipore). The transwell inserts were immediately placed back in the incubator after each measurement.

The impedance spectra were recorded by applying a sinusoidal waveform voltage of 20 mV$_{rms}$ using an LCR meter (ZM2731, NF) connected to the MPS through electrical feed-throughs and USB cables (ESI Fig. 1A†). The MPS was placed in the incubator during the measurement.

The equivalent circuit model consists of electrode impedance (Z_1, Z_2, Z_3, and Z_4), medium resistance (R_a and R_b), TEER (R) and tissue capacitance (C). Z_1, Z_2, Z_3, and Z_4 include impedance of the electrode-medium interface, wiring resistance, and contact resistance (Fig. 1G). As depicted in the equivalent circuit model of Fig. 1H, each measured impedance includes the total impedance, resistance and capacitance components present in their respective paths. The total impedance between electrode pairs was denoted as Z_{i-j} with i and j referring to the electrode numbers as illustrated in Fig. 1H, namely electrodes 1-2, 3-4, 1-4, and 2-3.

Typical impedance spectra for the two electrode pairs through the porous membrane are shown in Fig. 1I. However, R and C cannot be extracted due to the impedance of the electrodes, Z_i (i = 1, 2, 3, 4), and resistance of media, R_a and R_b. To eliminate them, the impedance of the epithelial tissue layer was measured from the difference of impedance between the two models in Fig. 1H. Then, the impedance can be expressed as

$$Z = \frac{(Z_{1-4} + Z_{2-3}) - (Z_{1-2} + Z_{3-4})}{2} \quad (1)$$

Therefore, the resulting R and C are derived as follows (ESI Note 1†):

$$R = \frac{(\mathrm{Re}\{Z\} - (R_a + R_b))^2 + \mathrm{Im}(Z)^2}{\mathrm{Re}\{Z\} - (R_a + R_b)} \quad (2)$$

$$C = -\frac{\omega \cdot \mathrm{Im}\{Z\}}{(\mathrm{Re}\{Z\} - (R_a + R_b))^2 + \mathrm{Im}\{Z\}^2} \quad (3)$$

in which ω (= $2\pi f$) is the angular frequency. The total medium resistance ($R_a + R_b$) between the electrodes in a blank device containing REGM was measured before cell seeding. The impedance was measured as averaged values obtained from 100 Hz to 1000 Hz, where both R and C contribute to Z before C becomes conductive (Fig. 1J).[29]

To facilitate comparisons with other systems, R was multiplied, and capacitance was divided by the culture area. RPTECs were cultured up to day 10 until maturation as indicated by the plateau observed in the TEER profiles (ESI Fig. 2†). During the culture time, REGM was refreshed every other day by manually flushing with a pipette. Impedance was measured automatically on a daily basis. After maturation, RPTECs in the devices were treated with cisplatin, cimetidine, or the vehicle control solution.

2.5. Immunocytochemistry

RPTECs were fixed in the devices by immersing them in a 4% paraformaldehyde solution (PFA, 43368, ALF) at room temperature for 15 min. The tissues were permeabilized in PBS (20012027, Gibco) containing 0.05% Triton-X (T8787-50ML, Sigma) at room temperature for 15 min for ZO-1 (33-9100, Thermo Fisher Scientific), OCT2 conjugated with Alexa Fluor 647 (ab205482, abcam), and LRP2 (ab76969, Abcam) samples and methanol at −20 °C for 10 min for CLDN2 (32-5600, Thermo Fisher Scientific) samples. The samples were blocked in PBS containing 10% donkey serum (S30-100ML, Merck Millipore) at room temperature for 90 min. After the samples were incubated with primary antibodies overnight at 4 °C, they were incubated in the secondary antibody conjugated with Alexa Fluor 488 (A-21202, Thermo Fisher Scientific) for the ZO-1 or CLDN2 samples, or Alexa Fluor 647 (A-31573, Thermo Fisher Scientific) for the LRP2 sample and DAPI (D3571, Thermo Fisher Scientific) for all the samples for 90 min at room temperature.

Microscopy was performed using an Olympus laser confocal microscope (FV3000, Olympus). RPTEC-laden membranes were cut out of the device and mounted on a coverslip. An anti-fade solution (S36937, Invitrogen) was applied.

2.6. Assessment of the association between TEER and the expression of tight junction proteins in cisplatin-induced nephrotoxicity

To examine the effects of cisplatin, REGM in the apical channel was replaced with REGM containing 100 μM cisplatin or the vehicle control solution. After administration, TEER values were monitored every 2 h for a total duration of 120 h. In parallel, immunostaining of ZO-1 and CLDN2 was performed.

2.7. Assessment of the association between the cell layer state and the impedance

The REGM in the basal channel was replaced with REGM including a CellEvent™ caspase 3/7 green detection reagent (CellEvent, C10423, invitrogen) and 100 μM cisplatin. After administration, the devices were incubated in a stage top incubator (INUB-ONICS-F1-MX, TOKAI HIT) with 5% CO$_2$ and at 37 °C. Imaging was performed using FV3000 at λ_{ex} = 488 nm and λ_{em} = 530 nm, while conducting impedance measurements simultaneously.

2.8. Image analysis

The cell perimeters indicated by ZO-1 and their internal area in immunofluorescence z-stack images of RPTECs on days 2, 4, 6, and 10 were measured with Fiji function "analyze particles" (NIH).[30] The perimeters were then divided by the area of each cell.

The number of detached cells was measured by counting the number of caspase 3/7-positive cells which were moved at least 13 μm (being the averaged diameter calculated from the area indicated by ZO-1 on day 10 as a circle (data not shown)) from the fluorescence z-stack images of RPTECs stained with CellEvent (ESI Movie 1†). The trajectory of each cell was measured using Fiji plugin TrackMate (ESI Movie 2†).[31,32] In addition, the number of caspase 3/7-positive cells was counted using Fiji function "analyze particles". Each value was divided by the culture area in each image.

2.9. Measurement of impedance to assess the cisplatin-induced toxicity of the RPTEC monolayer

To assess the effect of cisplatin concentration, REGM in the apical channel was replaced with REGM containing 10 μM or 50 μM cisplatin. To assess the effect of the inhibitor, the REGM in the basal channel was replaced with REGM containing 50 μM cisplatin and 1 mM or 10 mM cimetidine. The REGM in the basal channel was replaced with REGM containing 100 μM cisplatin. To assess the effect of cell polarity, the results were compared with those in the apical channel shown in section 2.6. After administration, the impedance was measured every 2 h for 120 h. In parallel, immunostaining of ZO-1 was performed.

3. Results

3.1. Comparison of the PT-MPS and conventional TEER measurement systems through evaluation of the RPTEC monolayer maturation process

The cell boundaries indicated by ZO-1 changes from a straight to zigzag shape with maturation (Fig. 2A). The averaged cell perimeters indicated by ZO-1 per unit area were found to increase from 0.55 μm μm^{-2} on day 2 to 0.72 μm μm^{-2} on day 4. However, the perimeter did not increase significantly from days 4 to 10 (0.79 μm μm^{-2}) (Fig. 2B).

The TEER of the RPTEC monolayer gradually increased during the first few days after seeding in both systems with ERS-2 (Fig. 2C) and the PT-MPS (Fig. 2D). The averaged TEER reached a plateau of about 44 Ω cm^2 after 3.4 days in ERS-2 (ESI Fig. 2A†) and 37 Ω cm^2 after 7.6 days in the PT-MPS (ESI Fig. 2B†). The capacitance increased until about day 3 with large variations, reaching a plateau of about 1.3 μF cm^{-2} (Fig. 2E).

The averaged coefficients of variation of the TEER on day 10 were 0.22 in the ERS-2 and 0.01 in the PT-MPS (Fig. 2C and D). The coefficients of variation of the averaged TEER on day 10 were 0.08 in ERS-2 and 0.21 in the PT-MPS (ESI Fig. 2†).

3.2. Association between the increase in TEER values and the expression of tight junction proteins during cisplatin-induced nephrotoxicity; the barrier kinetics

The time-course of TEER normalized by the initial value prior to cisplatin administration is plotted along with the vehicle control conditions (Fig. 3A). Following cisplatin administration at $t < 0$ h, the TEER immediately increased to 1.55 at the first time point of $t = 0$ h and decreased to 1.31 at $t = 2$ h. Then, it reached the peak value of 1.74 at $t = 14$ h and decreased to zero at $t = 90$ h. In the control experiment, after the drastic TEER increase to 1.74 at $t = 0$ h it also decreased to 1.07 at $t = 8$ h. It again gradually increased to 1.23 at $t = 20$ h and then slightly decreased to 0.83 at $t = 120$ h. In immunofluorescence images, ZO-1 and CLDN2 were found to be localized at cell–cell boundaries before cisplatin administration. At $t = 14$ h after 100 μM cisplatin administration, CLDN2 disappeared from the tight junction, but ZO-1 was still localized at the cell–

cell boundary. At $t = 120$ h, both ZO-1 and CLDN2 disappeared, and the number of nuclei obviously decreased compared to that at time $t = 120$ h after the vehicle control solution administration. On the other hand, at $t = 14$ h or $t = 120$ h after the vehicle control solution administration, both CLDN2 and ZO-1 were still localized at the cell–cell boundary (Fig. 3B). According to this result, we plotted capacitance and TEER by defining $t = 0$ h when the peak value was measured as shown in Fig. 4 and 5.

3.3. Association between the state of cell monolayers and the impedance

From $t = 0$ h to 18 h, the number of caspase 3/7-positive cells gradually increased (Fig. 4A). While the cumulative number of detached caspase 3/7-positive cells per unit area increased and reached 84 cells per mm^2 at $t = 18$ h, the capacitance also increased (Fig. 4B). Furthermore, along with the increase of the number of caspase 3/7-positive cells, the TEER decreased. The negative correlation was $r = -0.987$ (Fig. 4C). According to this result, we plotted capacitance and TEER until the capacitance increase was probed as illustrated in Fig. 5. In ESI Fig. 3,† we plot capacitance and TEER including the values before the peak and after capacitance increase.

3.4. Measurement of TEER and capacitance enables the assessment of cisplatin-induced toxicity in RPTEC monolayers

The dependency of capacitance and TEER on the cisplatin concentration was monitored (Fig. 5A). In the 10 μM cisplatin administration into the apical channel, the capacitance remained stable for over 94 h, and the TEER decreased to 0.81 as compared to the peak value at $t = 94$ h (green curve in Fig. 5A). Increasing the concentration of cisplatin to 50 μM resulted in a more rapid increase in capacitance and decrease in TEER at $t = 40$ h (yellow curve in Fig. 5A).

The capacitance increase and TEER decrease were monitored in the presence of cimetidine (Fig. 5B). The treatment of either 1 mM or 10 mM cimetidine in the basal channel inhibited the capacitance increase and TEER decrease caused by 50 μM cisplatin. Furthermore, more prominent inhibition effects of the capacitance increase and the TEER decrease were observed when 10 mM cimetidine was used compared with the 1 mM case (Fig. 5B). In the case of 1 mM cimetidine, the capacitance increased rapidly, and the TEER decreased to 0.63 at $t = 74$ h (light blue curve in Fig. 5B). In contrast, in the case of 10 mM cimetidine, the capacitance remained stable for over 88 h and the TEER decreased to 0.14 at $t = 74$ h (pink curve in Fig. 5B). Immunostaining at $t = 88$ h also shows less expression of ZO-1 in the case of 1 mM cimetidine and 50 μM cisplatin compared with the case of 10 mM cimetidine (Fig. 5C). To assess the dependency of capacitance and TEER on the apical or basal application of cisplatin, the case of the 100 μM cisplatin administration into the basal channel was compared with that of 100 μM cisplatin administration into the apical channel shown in the blue curve in Fig. 3A (Fig. 5D). Upon 100 μM cisplatin administration into the apical channel, the
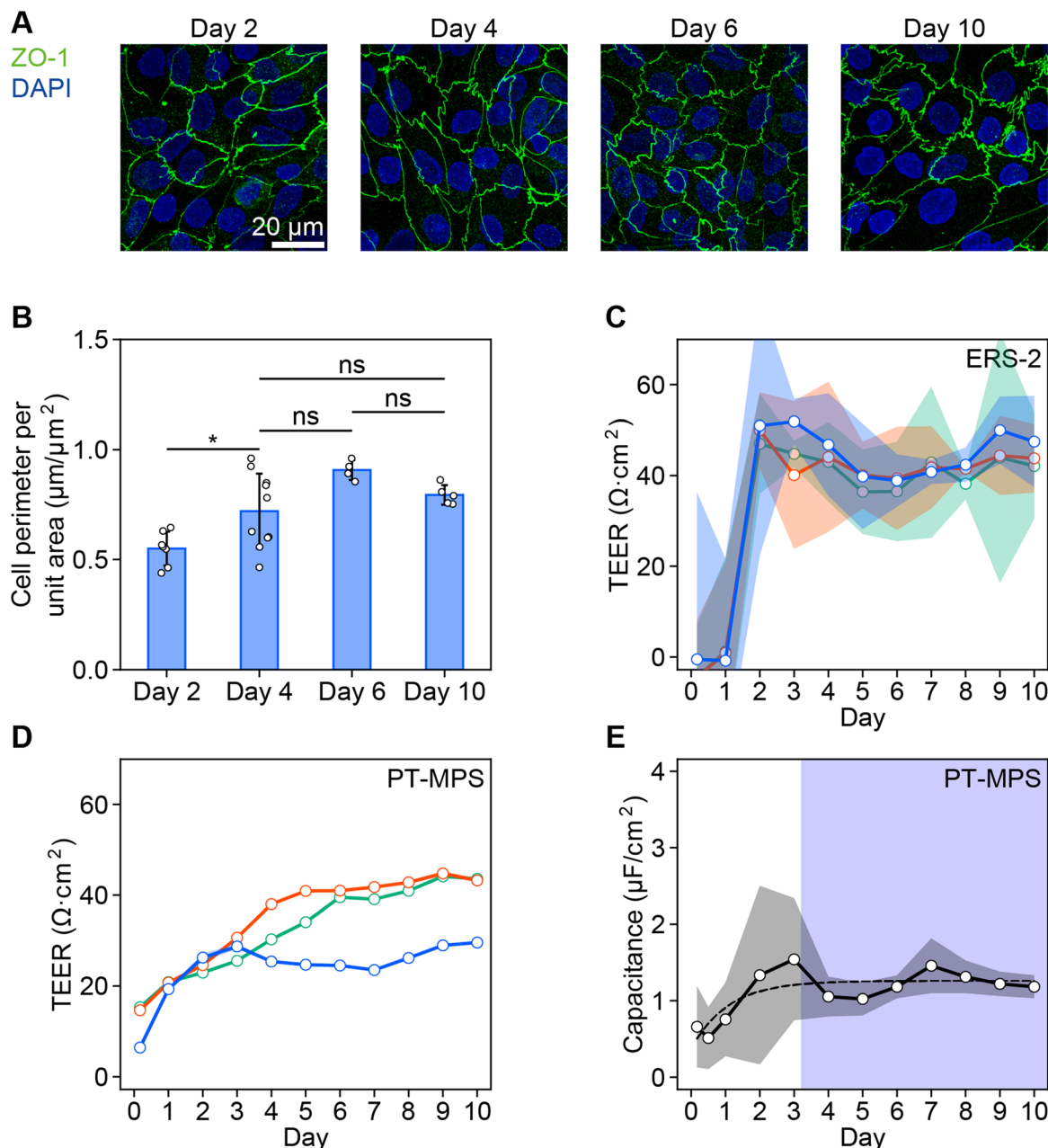
Fig. 2 Time course of maturation of RPTEC monolayers cultivated in the PT-MPS and in transwell inserts. A. Fluorescence z-stack images of RPTECs in the PT-MPS stained with ZO-1 (green) on days 2, 4, 6, and 10. Nuclei counter-stained with DAPI (blue). Scale bar = 20 μm. B. Quantification of the cell perimeter per unit area measured from the structure of the z-stack images of ZO-1 as shown in panel A. Tukey–Kramer's multiple comparison test. *p < 0.05. ns indicates no significant difference. Values out of the interquartile range were excluded as outliers. C. Evolution of TEER with time for three transwell inserts, measured with ERS-2. The shaded color bands represent the measurement error (n = 3 replicate measurements). D. TEER profile of the PT-MPS devices. The values are marked with the shaded color bands as measurement errors. But the bands are very small and hidden (n = 5 replicate measurements). E. The averaged capacitance measured simultaneously with TEER (D) (N = 3 devices). The shaded color bands represent the variation among devices. Curves were fit to the data using an exponential formula in the form of $A(t)$ = a + b × e$^{-t/\tau}$, where A represents capacitance at $t = \infty$, t is the time, a and b are fitting parameters, and τ is the time constant. The stability point is declared to be 3τ = 3.2 days. The blue colored region represents the stable state beyond the stability point.

capacitance increased at t = 38 h, and the TEER decreased gradually to 0.76 at t = 16 h (blue curve in Fig. 5D). In contrast, upon 100 μM cisplatin administration into the basal channel, the capacitance increased rapidly, and the TEER exhibited a significant drop to 0.17 at t = 16 h (red curve in Fig. 5D). In the

100 μM cisplatin administration into the apical channel, ZO-1 lost its complexity and had a linear staining pattern at the cell boundaries at t = 16 h. In contrast, in the 100 μM cisplatin administration into the basal channel, ZO-1 expression diminished significantly at t = 16 h (Fig. 5E).
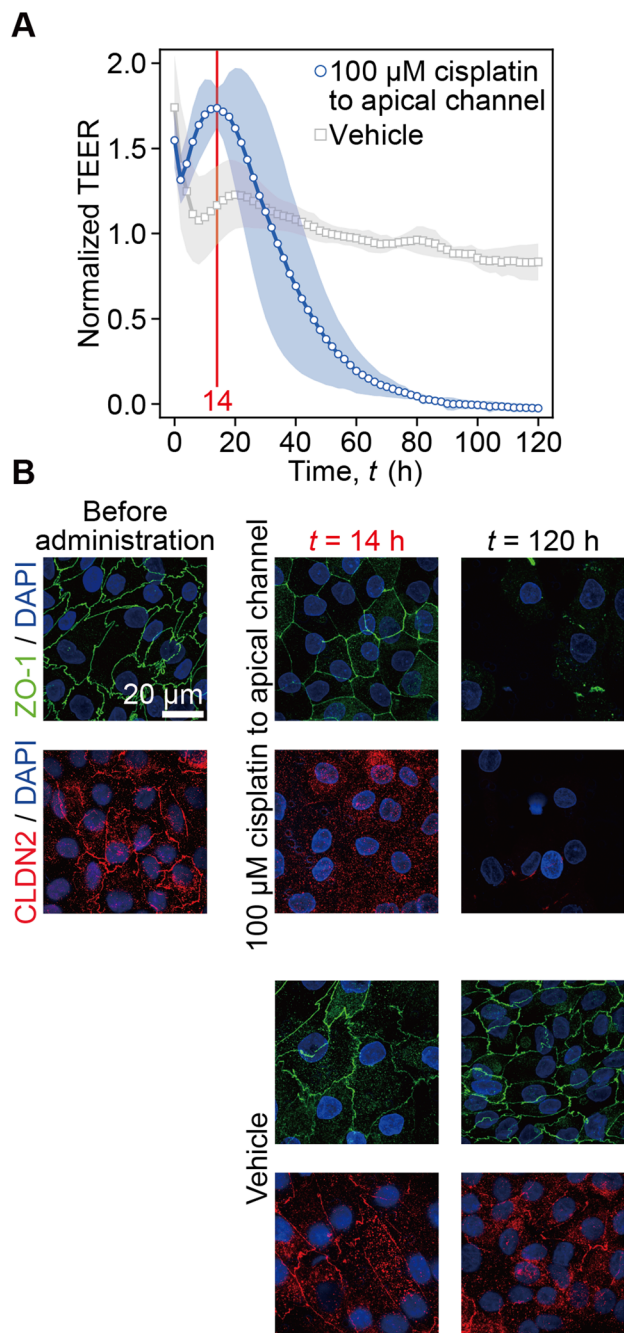
Fig. 3 Effects of cisplatin on RPTEC monolayers. A. TEER profiles recorded during 100 µM cisplatin administration to the apical side of RPTECs (blue curve) and vehicle control conditions without cisplatin administration (gray curve). The red line at $t = 14$ h represents the point at which the TEER curve reaches the peak value. The TEER values were normalized by the values before the cisplatin administration ($N = 3$ devices). B. Fluorescence z-stack images of RPTECs stained with ZO-1 (green) and CLDN2 (red) right before administration ($t < 0$), at $t = 14$ h, and at $t = 120$ h, after the cisplatin administration and the vehicle control solution administration. Nuclei are counter-stained with DAPI (blue). Scale bar = 20 µm.
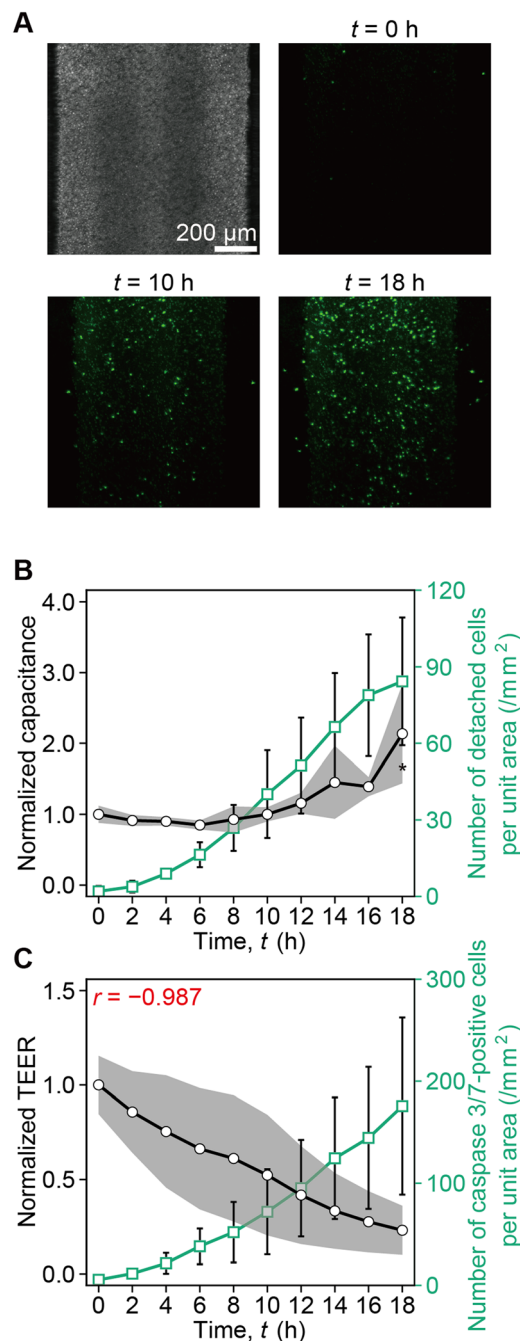

Fig. 4 Real-time monitoring of caspase 3/7 activation, capacitance, and TEER, during 100 µM cisplatin and CellEvent™ caspase-3/7 administration to the basal side of the RPTEC monolayers. A. Differential interference contrast observation z-stack image of RPTECs on the membrane and fluorescence z-stack images of caspase 3/7-positive RPTECs (green) stained with CellEvent™ caspase-3/7 at $t = 0$ h, $t = 10$ h, and $t = 18$ h. Scale bar = 200 µm. B. Evolution of capacitance with time (black curve), together with the cumulative number of detached caspase 3/7-positive cells per unit area measured from the images (green curve). Statistical significance between the average of cumulative values and the following value was assessed by unpaired two-tailed Student's t-test after F test ($N = 3$ devices). *$p < 0.05$. C. Evolution of TEER with time (black curve) together with the number of caspase 3/7-positive cells per unit area (green curve). The sample correlation coefficient r is -0.987. $N = 3$ devices. The capacitance and TEER values were normalized to their corresponding values at the time the TEER was maximum.
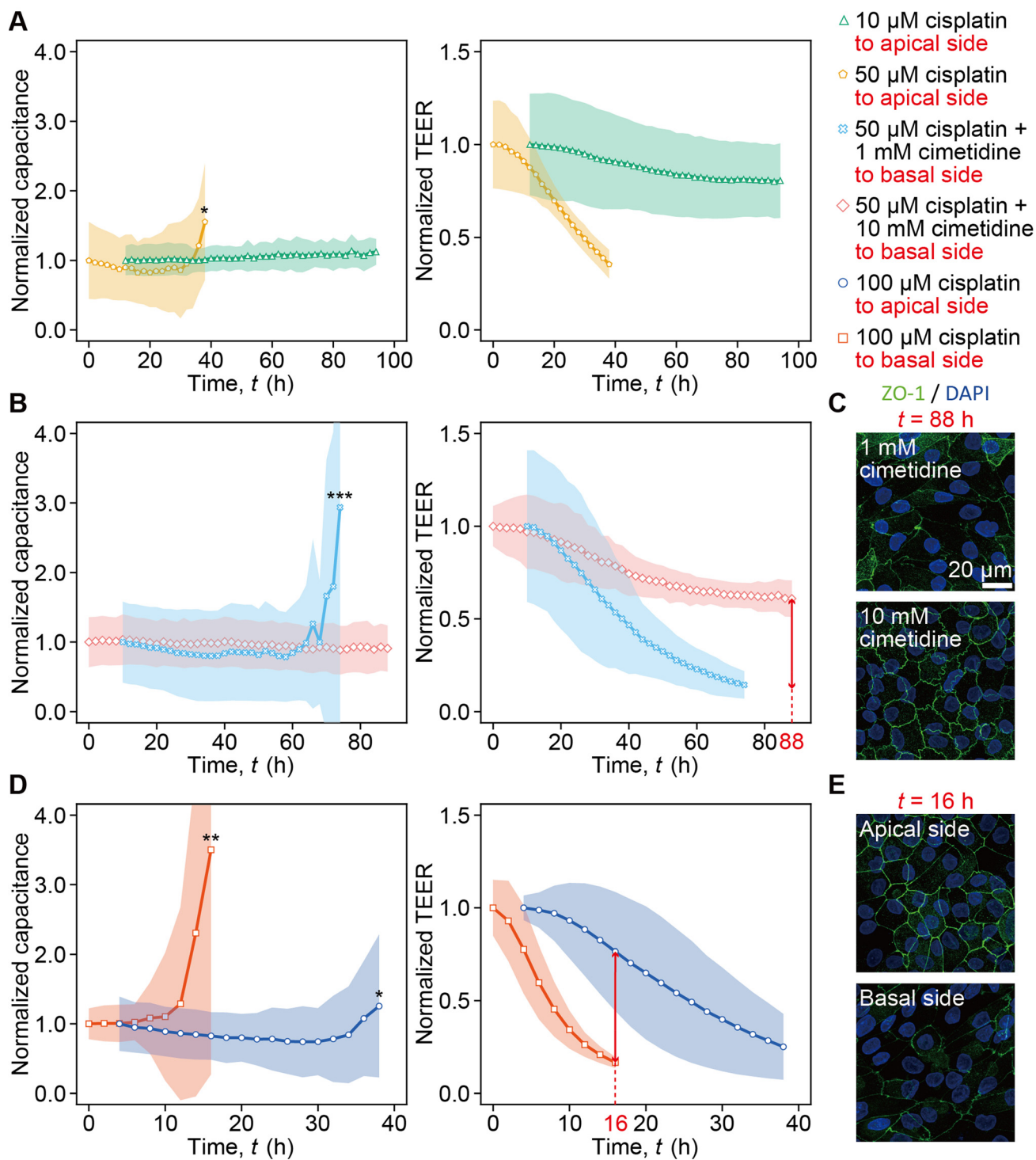
Fig. 5 Real-time monitoring of impedance upon cisplatin administration on RPTEC monolayers before the point of increase in capacitance. A. Capacitance and TEER values of RPTECs treated with 10 μM (N = 3 devices) or 50 μM (N = 4 devices) cisplatin at the apical side. B. Capacitance and TEER of RPTECs treated with 50 μM cisplatin with co-treatment of either 1 mM cimetidine (N = 3 devices) or 10 mM cimetidine (N = 4 devices) at the basal side. C. Appearance of ZO-1 (green) in RPTECs stained at t = 88 h. The samples were treated with 50 μM cisplatin and cotreated with cimetidine either at 1 mM or 10 mM. D. Capacitance and TEER profiles of RPTECs treated with 100 μM cisplatin applied to the apical side (N = 7 devices) and basal side (N = 3 devices). E. Appearance of ZO-1 (green) in RPTECs treated with 100 μM cisplatin applied to the apical or basal side at t = 16 h. Nuclei counter-stained with DAPI (blue). Scale bar = 20 μm. The capacitance and TEER were normalized by their corresponding values at the time the TEER was maximum. Statistical significance between the average of cumulative values and the subsequent value was assessed by the unpaired two-tailed Student's t-test after F test. *p < 0.05, **p < 0.01, and ***p < 0.001.

4. Discussion

ITO was selected as an electrode material (Fig. 1A and C), because it has long-term stability in culture medium and transparency at visible wavelengths (>80%) that enables microscopic cell observation even with electrodes covering the entire culture area (Fig. 1E). Covering the entire culture area by ITO electrodes also contributes to the creation of a uniform electric field, in which the equipotential plane is parallel to the cell layer (ESI Fig. 4†).

We proposed using two-pairs of electrodes in apical and basal channels and modeled the equivalent circuit incorporating the cell monolayer composed of R and C (Fig. 1G). The impedance was measured four times between electrodes, namely 1-2, 3-4, 1-4, and 2-3 (Fig. 1H). Using the equations presented in the experimental section, the contribution of the impedance of the electrode portion was eliminated in real time (Fig. 1I and J).

The impedance values measured using our PT-MPS setup were compared with the conventional well-established measurement using ERS-2. The ZO-1 expression at the boundary of cells was elevated until day 4, which indicates that the epithelial tissue matured to have tightness and a changed structure by at most day 4 (Fig. 2A and B). It corresponds to the capacitance increase and saturation at day 3.2 (Fig. 2E). The gradual TEER increase measured with the PT-MPS indicates the monitoring of barrier function development that cannot be detected using ERS-2. The PT-MPS had a larger variation of TEER among devices than that measured with ERS-2, but a much small variation in a device (Fig. 2C and D). The variation among PT-MPS devices is attributed to the variation of the effective cell culture area, which was brought about by differences among devices fabricated by a manual bonding process between the porous membrane and PDMS sheets. The TEER saturated by day 7.6, which indicates that the barrier function is fully developed under the culture conditions (ESI Fig. 2B†). Therefore, we cultured RPTECs up to day 10 in the cisplatin-induced toxicity experiments.

The increase of TEER to 1.74 at $t = 14$ h after exposing a matured RPTEC monolayer to cisplatin can be explained by ZO-1 and CLDN2 expression (Fig. 3). Owing to the medium change, it takes 5.4 h with RPTECs and 0.9 h without RPTECs after the increase of TEER to 1.46 and to 1.04, respectively (ESI Fig. 5†), which means that we are not able to properly assess the cisplatin toxicity until the TEER stabilized after the medium change. According to this, we focused on the dynamics after the second peak of TEER to discuss the effects of cisplatin. Cisplatin did not change ZO-1 expression but decreased CLDN2 expression at $t = 14$ h (Fig. 3B). Because CLDN2 is one of the transmembrane tight junction proteins that forms paracellular ion pores, higher CLDN2 expression contributes to lower TEER.[33] Thus, lower expression of CLDN2 at $t = 14$ h resulted in higher TEER than that before cisplatin administration, although ZO-1 expression was retained. The decrease of CLDN2 expression cannot sorely explain the increase in TEER because the multiple claudins form ion pores.[34] These indicate that the TEER measurement of PT-MPS detected the kinetics of the degradation of tight junctions by losing ion pores even while the tight junction was retained until $t = 14$ h, and then started to detect the damage of the tight junction after $t = 14$ h by cisplatin administration. This was the reason why we plotted capacitance and TEER after the appearance of the peak shown in Fig. 4 and 5. At $t = 120$ h, tight junctions were lost, and then some cells detached by the damage.

The importance of real-time measurement of TEER and capacitance to distinguish the epithelial tissue maturation, toxicological damage, and cell detachment is supported by monitoring ZO-1 expression and caspase 3/7-positive cells, which can be explained by four stages. (1) After the cell seeding, TEER increases with the barrier function development because the cells completely cover the porous membrane, and the capacitance slightly increases to a constant value without fluctuation as the cell membrane surface area increases (Fig. 2). (2) After the tissue maturation, TEER and capacitance remain stable. (3) Once cisplatin is administered, TEER decreases as apoptosis is damaged, while capacitance does not significantly increase after the temporary TEER increase. (4) After cell detachment, the capacitance increases significantly because the equivalent circuit model would no longer be valid. Owing to this process, the impedance reflects the tissue tightness until the significant increase of capacitance caused by the cell detachment. To assess the impedance of tissue layer, we plotted capacitance and TEER before the capacitance increase as shown in Fig. 5.

With 50 μM cisplatin, the abrupt capacitance increase was measured at $t = 38$ h, while TEER started to decrease after the initial peak and reached 0.35 by $t = 38$ h. This indicates that the cell detachment was not detected until $t = 38$ h, but the barrier disruption was detected by TEER even at $t < 38$ h. In contrast, with 10 μM cisplatin the capacitance did not change significantly owing to the absence of cell detachment; however, TEER gradually decreased to 0.81 (Fig. 5A), which was nearly identical to the value at $t = 120$ h after vehicle control solution addition (Fig. 3A). This demonstrates no barrier damage at the 10 μM cisplatin concentration. The simultaneous measurement of capacitance and TEER enabled us to terminate the measurement when the cells detached, *i.e.*, at $t = 38$ h for 50 μM cisplatin.

The weakened cytotoxicity with increasing cimetidine concentration from 1 mM to 10 mM was monitored (Fig. 5B). With 1 mM cimetidine, cell detachment was monitored at $t = 74$ h by the capacitance increase, while TEER kept decreasing and reached 0.14 owing to the barrier disruption. With 10 mM cimetidine, TEER gradually decreased until $t = 88$ h without capacitance increase. The ZO-1 expression correlates the capacitance and TEER measurement, because it is maintained to a greater extent with 10 mM cimetidine at $t = 88$ h (Fig. 5C).

Transporter-dependent cytotoxicity by cisplatin was monitored (Fig. 5D). Cisplatin administration into the basal channel, where OCT2 is expressed, caused the drastic capacitance increase at $t = 16$ h and TEER also decreased steeply.

However, when cisplatin was administered to the apical channel, where LRP2 is expressed, cell detachment was not detected until t = 38 h, and TEER decreased gradually. The ZO-1 expression at t = 16 h (Fig. 5E) demonstrated that the cytotoxicity by administration into the basal channel was stronger, corresponding to the capacitance and TEER results.

5. Conclusion

We established a two-channel MPS for measuring the impedance of proximal tubule epithelial layers in real time. By integrating two pairs of ITO electrodes, uniform electric fields over the cell layer could be produced. The effect of the electrode portion was eliminated using the results of four times measurements with these four electrodes. The capacitance and TEER, if analyzed concurrently, enable the detection of cell detachment and the kinetics of the barrier function derived from tight junction-associated proteins, respectively. Cisplatin-induced nephrotoxicity could be accessed in a dose-dependent fashion demonstrating the sensitivity to the effect of cimetidine as an inhibitor and cell polarity. The methods introduced here are versatile and high throughput and can be applied to other device geometries. Measurement of capacitance and TEER profiles in tandem offers the potential of more predictive preclinical screenings.

Author contributions

Conceptualization, Y. T.; formal analysis, Y. T., methodology, Y. T.; investigation, Y. T.; writing – original draft, Y. T.; visualization, Y. T.; writing – review & editing. R. B. S. and R. Y.; supervision, R. B. S., K. F., and R. Y.; resources, R. Y.; and funding acquisition, R. Y.

Conflicts of interest

The authors have no conflicts of interest to declare.

Acknowledgements

References

1 B. Zhang, A. Korolj, B. F. L. Lai and M. Radisic, *Nat. Rev. Mater.*, 2018, **3**, 257–278.

2 H. Kimura, Y. Sakai and T. Fujii, *Drug Metab. Pharmacokinet.*, 2018, **33**, 43–48.

3 M. A. Perazella, *Clin. J. Am. Soc. Nephrol.*, 2018, **13**, 1897–1908.

4 J. Y. C. Soo, J. Jansen, R. Masereeuw and M. H. Little, *Nat. Rev. Nephrol.*, 2018, **14**, 378–393.

5 M. J. Wilmer, C. P. Ng, H. L. Lanz, P. Vulto, L. Suter-Dick and R. Masereeuw, *Trends Biotechnol.*, 2016, **34**, 156–170.

6 A. Wilmes, C. Bielow, C. Ranninger, P. Bellwon, L. Aschauer, A. Limonciel, H. Chassaigne, T. Kristl, S. Aiche, C. G. Huber, C. Guillou, P. Hewitt, M. O. Leonard, W. Dekant, F. Bois and P. Jennings, *Toxicol. in Vitro*, 2015, **30**, 117–127.

7 A. Single, H. Beetham, B. J. Telford, P. Guilford and A. Chen, *J. Biomol. Screening*, 2015, **20**, 1286–1293.

8 T. Gerasimenko, S. Nikulin, G. Zakharova, A. Poloznikov, V. Petrov, A. Baranova and A. Tonevitsky, *Front. Bioeng. Biotechnol.*, 2020, **7**, 1–11.

9 O. Y. F. Henry, R. Villenave, M. J. Cronce, W. D. Leineweber, M. A. Benz and D. E. Ingber, *Lab Chip*, 2017, **17**, 2264–2271.

10 S. Fuchs, S. Johansson, A. Tjell, G. Werr, T. Mayr and M. Tenje, *ACS Biomater. Sci. Eng.*, 2021, **7**, 2926–2948.

11 B. M. Maoz, A. Herland, O. Y. F. Henry, W. D. Leineweber, M. Yadid, J. Doyle, R. Mannix, V. J. Kujala, E. A. Fitzgerald, K. K. Parker and D. E. Ingber, *Lab Chip*, 2017, **17**, 2294–2302.

12 S. Chen, R. Einspanier and J. Schoen, *Histochem. Cell Biol.*, 2015, **144**, 509–515.

13 A. S. Ebrahim, T. Ebrahim, H. Kani, A. S. Ibrahim, T. W. Carion and E. A. Berger, *Sci. Rep.*, 2022, **12**, 14126.

14 S. Arndt, J. Seebach, K. Psathaki, H. J. Galla and J. Wegener, *Biosens. Bioelectron.*, 2004, **19**, 583–594.

15 H. Lohren, J. Bornhorst, R. Fitkau, G. Pohl, H. J. Galla and T. Schwerdtle, *BMC Pharmacol. Toxicol.*, 2016, **17**, 63.

16 H. Kavand, R. Nasiri and A. Herland, *Adv. Mater.*, 2022, **34**, 1–36.

17 M. A. U. Khalid, Y. S. Kim, M. Ali, B. G. Lee, Y. J. Cho and K. H. Choi, *Biochem. Eng. J.*, 2020, **155**, 107469.

18 X. Zhang, W. Wang, F. Li and I. Voiculescu, *Lab Chip*, 2017, **17**, 2054–2066.

19 J. Wegener, C. R. Keese and I. Giaever, *Exp. Cell Res.*, 2000, **259**, 158–166, 10942588.

20 J. W. Song, S. P. Cavnar, A. C. Walker, K. E. Luker, M. Gupta, Y. C. Tung, G. D. Luker and S. Takayama, *PLoS One*, 2009, **4**, e5756.

21 J. Yin and J. Wang, *Acta Pharm. Sin. B*, 2016, **6**, 363–373.

22 G. Ciarimboli, D. Deuster, A. Knief, M. Sperling, M. Holtkamp, B. Edemir, H. Pavenstädt, C. Lanvers-Kaminsky, A. A. Zehnhoff-Dinnesen, A. H. Schinkel, H. Koepsell, H. Jürgens and E. Schlatter, *Am. J. Pathol.*, 2010, **176**, 1169–1180.

23 R. P. Miller, R. K. Tadagavadi, G. Ramesh and W. B. Reeves, *Toxins*, 2010, **2**, 2490.

24 Y. Hori, N. Aoki, S. Kuwahara, M. Hosojima, R. Kaseda, S. Goto, T. Iida, S. De, H. Kabasawa, R. Kaneko, H. Aoki, Y. Tanabe, H. Kagamu, I. Narita, T. Kikuchi and A. Saito, *J. Am. Soc. Nephrol.*, 2017, **28**, 1783–1791.

25 M. Odijk, A. D. Van Der Meer, D. Levner, H. J. Kim, M. W. Van Der Helm, L. I. Segerink, J. P. Frimat, G. A. Hamilton, D. E. Ingber and A. Van Den Berg, *Lab Chip*, 2015, **15**, 745–752.

26 J. Yeste, X. Illa, C. Gutiérrez, M. Solé, A. Guimerà and R. Villa, *J. Phys. D: Appl. Phys.*, 2016, **49**, 375401.

27 A. Ozkok and C. L. Edelstein, *BioMed Res. Int.*, 2014, **2014**, 1–17.

28 T. Ludwig, C. Riethmüller, M. Gekle, G. Schwerdt and H. Oberleithner, *Kidney Int.*, 2004, **66**, 196–202.

29 K. Benson, S. Cramer and H. J. Galla, *Fluids Barriers CNS*, 2013, **10**, 1–11.

30 J. Schindelin, I. Arganda-Carreras, E. Frise, V. Kaynig, M. Longair, T. Pietzsch, S. Preibisch, C. Rueden, S. Saalfeld, B. Schmid, J. Y. Tinevez, D. J. White, V. Hartenstein, K. Eliceiri, P. Tomancak and A. Cardona, *Nat. Methods*, 2012, **9**, 676–682.

31 J. Y. Tinevez, N. Perry, J. Schindelin, G. M. Hoopes, G. D. Reynolds, E. Laplantine, S. Y. Bednarek, S. L. Shorte and K. W. Eliceiri, *Methods*, 2017, **115**, 80–90.

32 D. Ershov, M. S. Phan, J. W. Pylvänäinen, S. U. Rigaud, L. Le Blanc, A. Charles-Orszag, J. R. W. Conway, R. F. Laine, N. H. Roy, D. Bonazzi, G. Duménil, G. Jacquemet and J. Y. Tinevez, *Nat. Methods*, 2022, **19**, 829–832.

33 S. Amasheh, N. Meiri, A. H. Gitter, T. Schöneberg, J. Mankertz, J. D. Schulzke and M. Fromm, *J. Cell Sci.*, 2002, **115**, 4969–4976.

34 M. Fromm, J. Piontek, R. Rosenthal, D. Günzel and S. M. Krug, *Pflügers Arch.*, 2017, **469**, 877–887.